Solar Phys (2009) 255: 239–251
DOI 10.1007/s11207-009-9326-9

A New Method of Calibration of Photographic Plates from Three Historic Data Sets

Andrey G. Tlatov · Alexei A. Pevtsov · Jagdev Singh

Received: 17 November 2008 / Accepted: 16 February 2009 / Published online: 3 March 2009

Abstract We analyze the synoptic data taken in the Ca II K spectral line with spectroheliographs at Kodaikanal Observatory from 1907 to 1999, at Mount Wilson Observatory from 1915 to 1985, and at the National Solar Observatory at Sacramento Peak from 1963 to 2002. Photographic data were digitized and calibrated following the same set of procedures developed by the authors of this paper. Using calibrated data, we have outlined bright plages and have calculated a plage index defined as the fraction of solar hemisphere occupied by the chromospheric plages and enhanced network. We present a detailed description of our method and provide a brief comparison of Ca II K plage indices derived using data from these three historic data sets.

Keywords Solar cycle, observations · Chromosphere, active · Chromosphere, quiet

1. Introduction

Arguably, Ca II K line observations are the most readily available data from ground-based observatories to characterize long-term solar activity in ultraviolet radiation. Furthermore, in the absence of direct measurements, the Ca II K index can serve as a good proxy for solar magnetic flux (Ortiz and Rast, 2005). At the beginning of the 20th century several spectroheliographs were built to observe solar activity in the Ca II 3933.67 Å (Ca II K) line. Now, these various data sets represent a gold mine for studies of solar activity from the last

A.G. Tlatov
Kislovodsk Solar Station of Pulkovo Observatory, Kislovodsk, Russia
e-mail: tlatov@mail.ru

A.A. Pevtsov (✉)
National Solar Observatory, Sunspot, NM 88349, USA
e-mail: apevtsov@nso.edu

J. Singh
Indian Institute of Astrophysics, Koramangala, Bangalore, India
e-mail: jsingh@iiap.res.in

10 solar cycles or about 100 years. In the past, these data were used to derive plage area. The derivations were made manually by the observer, and hence they are subjective. The degree of subjectivity varies among the data sets and even within the same data set, making it difficult to combine data into a single uniform sequence (Foukal, 1996).

In this paper we describe a new method to reduce digitized photographic images of full-disk data taken in the Ca II K line. We apply the method to three different data sets and compare the calibrated data. We find a high correlation between all three data sets, which suggests that our processing routine can be used to combine these historic data into a single data set, thus enabling objective studies of properties of chromospheric plages, network elements, and ephemeral bright points. The rest of the paper is organized as follows: In Section 2 we provide details of our data reduction technique, with Section 2.4 describing the selection of plage areas. Section 3 summarizes our findings.

2. Data and Data Analysis

2.1. The Three Data Sets

We analyze photographic archives of three different spectroheliographs: the Kodaikanal Observatory in India (for a period of observation from 1907 to 1999; Makarov *et al.*, 2004), the National Solar Observatory at Sacramento Peak (1963 – 2002; Tlatov and Pevtsov, 2005) and the Mount Wilson Observatory (1915 – 1985; Lefebvre *et al.*, 2005) in the USA. Kodaikanal Observatory (KKL) images were acquired with an exit slit width of the spectroheliograph of 0.5 Å centered at $\lambda = 3933.67$ Å. The spatial resolution is approximately 1.2 arc seconds per pixel (and so the radius of the solar disk on KKL images is about 750 pixels). KKL images were digitized by us using a commercial flatbed 8-bit digitizer. The digital archive of Kodaikanal Ca II K observations contains 26 640 spectroheliograms obtained on 26 620 observing days.

Mount Wilson Observatory (MWO) data were recorded with a spectral bandpass of about 0.35 Å in width,[1] with a spatial resolution of about 2.8 arc seconds per pixel (and so the radius of the solar disk on MWO images is about 350 pixels). The data digitized with a 12-bit digitizer (Ermolli *et al.*, 2007) were accessed from the on-line archive at http://www.astro.ucla.edu. The Mount Wilson Observatory digital archive used in this study contains 34 166 images obtained on 20 684 observing days.

The National Solar Observatory at Sacramento Peak (NSO/SP) data were taken on a daily basis with a 0.514 Å exit slit centered at $\lambda = 3933.67$ Å. The spatial resolution of NSO/SP data is similar to that of KKL data (*i.e.*, about 1.2 arcseconds per pixel, so the radius of the solar disk on NSO/SP images is about 750 pixels). The digital archive of NSO/SP Ca II K observations contains 6033 daily images. In addition, 1138 images were taken with the exit slit offset by 0.38 Å to the red wing of the Ca II K line. In the present investigation, we only use data obtained at the Ca II K line center. NSO/SP images were digitized by the authors using a commercial flatbed 16-bit digitizer.

Owing to differences in exit slit width, images from different instruments may sample different portions of solar atmosphere. Ermolli *et al.* (2008) had pointed out that MWO images tend to show chromospheric filaments, whereas broader bandpass KKL and NSO/SP images have a tendency to show sunspots. Such differences in spectral response might affect the plage contrast, as discussed in Section 2.4.

[1] This width is obtained when the diffraction at the exit slit is taken into consideration (Bertello, 2008, private communication). Ermolli *et al.* (2008) have reported a 0.2 Å nominal exit slit.

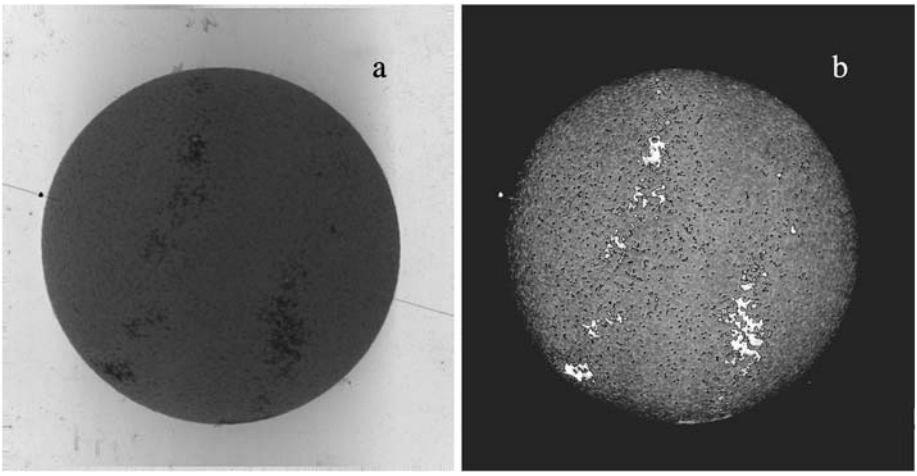

Figure 1 Example of (a) original (shown in negative) and (b) calibrated image of Kodaikanal spectroheliogram observed on 5 January 1908. Contours shown on panel (b) outline bright plage and enhanced network areas selected by our routine.

Figure 1a provides an example of a typical spectroheliogram from our KKL data set. The image shows a noticeable nonuniformity of scattered light across the field of view (compare background levels outside the solar disk) and spots on the film surface (*e.g.*, bright spots outside the limb). There are also a number of less noticeable issues, which are typical of all photographic film data (*e.g.*, caused by a nonlinear response function or a nonuniform sensitivity over the strip of film/photographic plate). In addition, the three instruments had different optical setups, which in some cases resulted in geometric distortions to the solar images. In earlier NSO/SP data, the geometric distortions vary among the images, perhaps as the result of instrument realignment in the attempt to improve the instrument performance. Also, some images do not have a calibration wedge imprinted on the photographic plate, which complicates their photometric calibration. [According to Ermolli *et al.* (2008), 75% of MWO images do not have wedges imprinted on the photographic plates. The fraction of KKL images without a wedge is somewhat lower than 55%, as reported by Ermolli *et al.* (2008). This is simply because, at the time of digitization, the wedge was often not included in the scanned area owing to its distant location relative to the main image.]

The reduction procedure that we have developed addresses many of these issues.

In the past, several methods were developed to reduce digitized Ca II K line images (*e.g.*, Foukal, 1996, 1998; Lefebvre *et al.*, 2005; Ermolli *et al.*, 2008). Given the nature of photographic data, these previous methods had to address the very same issues just listed. Ermolli *et al.* (2008) had provided a comprehensive review of issues typical for MWO, KKL, and other data sets of full-disk K line photographic observations. They had described elements of their data reduction procedure and compared various parameters derived from the data. However, as is typical for any data reduction, one cannot rely on a single technique. For example, techniques based on the assumption of removal of a constant background do not remove a nonuniform background as on Figure 1a. [Ermolli *et al.* (2008) do investigate the presence of large-scale image inhomogeneities on Ca II K images, but their technique does not remove these inhomogeneities.] Also, the variation in image contrast (*e.g.*, caused by off-band observations, properties of photographic film, or film development irregularities) may affect the determination of the solar limb, when a gradient-based method is used. In-

deed, Ermolli *et al.* (2008) had shown the presence of variations in image contrast in both photographic and (more modern) CCD observations of solar disk images taken in the Ca II K line. Our technique addresses some of these shortcomings.

Our analysis of spectrograms is divided into several major steps: identification of the solar limb and circularization of solar images, normalization of image intensities to create a sequence of calibrated images, calculation of center-to-limb function, and selection of bright plages. The following sections describe these steps in more detail.

2.2. Identification of Solar Limb and Image Circularization

In this step, we define the location of the solar limb, circularize the solar disk, and determine the correct image orientation (*i.e.*, the true solar North direction). First, we select an approximate disk center and measure the average intensity near the approximate disk center. Next, we divide the image (including all pixels both inside and outside the solar disk) into four quadrants with respect to a selected center point and calculate the intensity distribution in each quadrant using all pixels within this quadrant. Typically, the distribution function shows two maxima: One hump corresponds to pixels belonging to the solar disk, and the other to pixels outside the solar disk (background). The valley between these two peaks is taken as an initial intensity threshold corresponding to the Sun's limb, I_{limb}, in each quadrant. Variations in disk brightness and level of background across the image are taken into account by interpolating I_{limb} between quadrants. Finally, the coordinates of limb pixels are used to fit an ellipse following Xie and Ji (2002). If the eccentricity of the ellipse exceeds 0.13, the image is circularized. In practice, most NSO/SP and some KKL spectroheliograms had been circularized, but MWO images were not circularized.

To determine a true orientation of images, we first determined the solar P angle (the angle between the solar rotation axis and the Earth's rotation axis in the plane of the sky) using an approximate position of the solar North marked on each image by the observer. Next, we computed the solar P angle for the time of observations. If the difference between the observed and computed P angle was smaller than 10°, we used the computed P angle. For images with a larger difference, the P angle was determined interactively either using images observed on several consecutive days or by fitting known coordinates of active regions. The latter procedure was applied mostly to the NSO/SP data.

2.3. Normalization of Image Intensities

The next step of our image processing is to create a sequence of calibrated images. To photometrically calibrate photographic images, one needs to know the specific characteristic curve (of film) and the contribution of scattered light. Typically, the determination of the characteristic curve is done by using a calibration wedge imprinted on the photographic film. Unfortunately, some images (especially, earlier MWO data) lack the wedge imprint. To deal with this complication in a systematic manner, we have employed the following procedure.

We base our calibration method on the assumption that center-to-limb variation (CLV) in quiet Sun (*i.e.*, areas of the Sun without bright floccules) corresponds to a standard curve. We assume that this standard CLV curve is independent of the overall level of solar activity (Solanki, 2006, private communication), and we fit the standard CLV curve to the observed brightness, by minimizing the difference between the observed and standard CLV curves (see Figure 2).

The observed brightness on a photographic plate ($I_{\rm obs}$) can be defined as

$$I_{\rm obs} = (I_{\rm solar} + I_{\rm scatt}) \times \gamma + D, \tag{1}$$

where $I_{\rm solar}$ is true solar intensity, $I_{\rm scatt}$ is the contribution of scattered light from the spectral grating, γ is the film contrast, and D represents the combined contribution of fog level, scattered light from telescope optics feeding the spectroheliograph, and scattered light from Earth's atmosphere.

We determine γ, $I_{\rm solar}$, $I_{\rm scatt}$, and D via an iterative procedure. In these calculations, we assume that for typical quiet Sun intensities, contrast γ is constant across each plate, and $I_{\rm solar}$ follows a standard CLV curve, $I_{\rm ST}$ (Pierce and Slaughter, 1977), given by

$$I_{\rm ST}(\lambda, \xi) = a(\lambda) + b(\lambda)\xi + c(\lambda)\xi^2, \tag{2}$$

where λ is the wavelength, $\xi = \ln[\cos(\theta)]$, and $\mu = \sin(\theta)$. For the spectral range near the Ca II K line, $a = 1.0$, $b = 0.66030$, and $c = 0.13914$ (Pierce and Slaughter, 1977).

Then, γ, $I_{\rm solar}$, $I_{\rm scatt}$, and D can be determined by fitting the standard CLV ($I_{\rm ST}$) to the observed profiles only at two points: For $I_{\rm real} = I_{\rm obs} - D = \gamma \cdot (I_{\rm ST} + I_{\rm scatt})$, one can write

$$\frac{I_{\rm real}(\mu_0)}{I_{\rm real}(\mu_1)} = \frac{I_{\rm ST}(\mu_0) + I_{\rm scatt}}{I_{\rm ST}(\mu_1) + I_{\rm scatt}}, \tag{3}$$

where μ_0 and μ_1 are heliocentric distances at two fixed positions. Typically, we select $\mu_0 = 0$ and $\mu_1 = 0.9$.

Then

$$I_{\rm scatt} = I_{\rm ST}(\mu_0) \frac{I_{\rm obs}(\mu_1) - I_{\rm real}(\mu_0) \cdot I_{\rm ST}(\mu_1)/I_{\rm ST}(\mu_0)}{I_{\rm real}(\mu_0) - I_{\rm real}(\mu_1)} \tag{4}$$

and

$$\gamma = \frac{I_{\rm real}(\mu_0)}{I_{\rm ST}(\mu_0) + I_{\rm scatt}}. \tag{5}$$

The fitting is done in several iterations. First, D is assumed to be zero, and $I_{\rm ST}$ is fitted to the observed CLV profile (Figure 2). Next, Equations (3) – (5) are solved for $I_{\rm scatt}$ and γ, and Equation (1) is used to determine a new D. This procedure is repeated until converging solutions for all five parameters are found. Typically, convergence is achieved after a small number of iterations (one to three). After fitting is completed, $I_{\rm scatt}$, γ, and D are used to calibrate the images. Figure 1b gives an example of a calibrated solar disk image.

Comparing the observed and fitted center-to-limb profiles on Figure 2 one can notice that the scanned image shows large-scale variations in intensity most likely due to the presence of bright plages and scattered light. The calibrated image (Figure 1b) is more uniform in its large-scale intensity distribution. Also, fitting the standard CLV curve appears to overestimate the limb darkening (cf. the solid and dashed lines near the solar limb, $\mu > 0.8$, Figure 2). This might result in a slight increase in brightness of plages near the solar limb.

2.4. Allocation of Plages

In this step, we calculate a center-to-limb variation for calibrated images, and determine boundaries of bright plages using the CLV as an approximation for a quiet Sun intensity. The technique is similar to the method of determination of quiet Sun level described in Section 2.2. First, the solar disk is divided into four sectors. For each sector, we build the

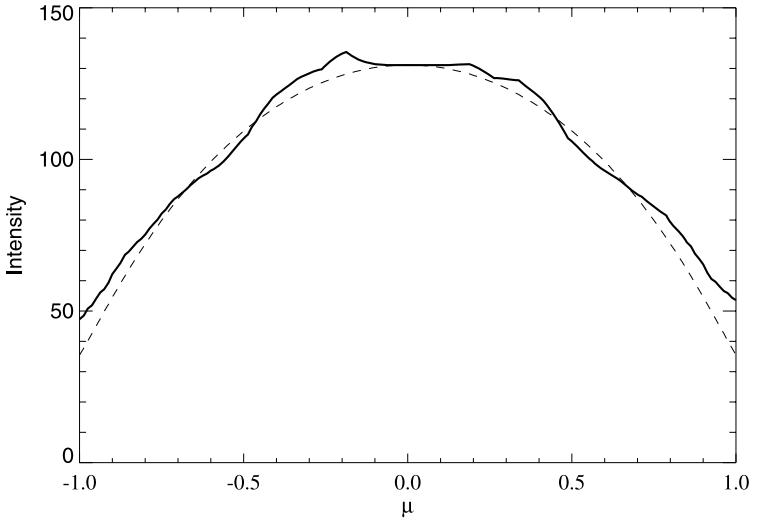

Figure 2 Average profile of a "quiet Sun" intensity for image shown on Figure 1 (thick solid line, with only North – South slice shown). The dashed line is the standard center-to-limb brightness fitted to the observed profile.

distribution of pixels by their intensity and determine the maximum of this distribution, $I_{\max}$, and its standard deviation, σ. All pixels whose intensity exceeds $I_{\max}+3\sigma$ are excluded from further calculation of the CLV. The remaining pixels are included as quiet Sun pixels for the following iterations. At the next iteration, each segment is divided in half (both in position angle and radial distance from the disk center in the polar coordinate system), and previous steps are repeated. We stop iterating when the number of segments (both in position angle and in radial distance) reaches 16, or when the number of pixels remaining in each segment drops below a pre-set number (sufficient to build a statistically meaningful distribution). When the final segmentation is reached, pixels classified as quiet Sun in each segment are averaged, and this average intensity is designated as the quiet Sun ($I_{\rm QS}$) level for the center of the segment. Finally, $I_{\rm QS}$ intensities between segments are interpolated to all pixels of solar disk using a cubic spline.

Since the area near the disk center ($\mu \leq 0.3$) is too small for segmentation, we used a different approach. First, the average intensity inside a $\mu \leq 0.3$ circle is calculated, and it is used as the quiet Sun level at the disk center, $I_{\rm QS}(\mu = 0)$. For pixels within $0 < \mu \leq 0.3$, the quiet Sun level is determined as

$$I_{\rm QS}(\mu) = I_{\rm QS}(0) + \mu\big[I^{\rm s}_{\rm QS}(\mu) - I_{\rm QS}(0)\big], \tag{6}$$

where $I^{\rm s}_{\rm QS}(\mu)$ is the quiet Sun level from a spline approximation. This procedure ensures that quiet Sun in the central area of the solar disk and $I_{\rm QS}$ determined by segmentation are merged together.

After the quiet Sun level is determined, one can define bright plages by using a fixed threshold relative to a local brightness of quiet Sun $I_{\rm QS}(\mu)$ (*e.g.*, Makarov and Tlatov, 2002; Makarov *et al.*, 2004). However, we have found that plage contrast is systematically lower in Kodaikanal images as compared with the Mount Wilson Observatory data. [Figure 13 in Ermolli *et al.* (2008) indicates that, with the exception of pre-1930 years, KKL data exhibit higher image contrast as compared with MWO data. However, visual inspection of Figure 1

in Ermolli *et al.* (2008) indicates that KKL images have lower plage contrast relative to MWO data. Our conclusion about systematically lower plage contrast in KKL data is in agreement with Figure 1 in Ermolli *et al.* (2008), but not with their Figure 13.] In addition, all three data sets contain images with noticeably lower contrast as compared with other periods of the same data set (*e.g.*, Kodaikanal observations from 1940 to 1953). We speculate that the latter could be related to a shift of spectra away from the core of the Ca II K line (since, most likely, data are taken slightly off-band), whereas the former may be a consequence of the 8-bit digitization of Kodaikanal data, which reduces the dynamic range of scanned data. It is worth noticing that Ermolli *et al.* (2008) had also described occasional off-band observations, although they did not specify the data set (KKL or MWO). Also, the width of the exit slit of the spectroheliographs is different ($\delta \approx 0.35$ Å at Mount Wilson Observatory and $\delta \approx 0.5$ Å for Kodaikanal and NSO/SP), which might affect the plage contrast as well (owing to the contribution of the Ca II K wings, whose height formation extends to the photosphere). Thus, instead of using a fixed threshold, we define plages ($I_{\rm plage}$) on the basis of the distribution of brightness of pixels above the local quiet Sun area and the full width at half-maximum (FWHM, or Γ) of this distribution: $I_{\rm plage} \geq I_{\rm QS}(\mu) + C \cdot \Gamma$. From the experiment, we have established that $C = 1.5$ works well for all three data sets. It is worth noting that the histogram method offers a significant improvement over the simple threshold method. Because the threshold method is sensitive to image contrast, any variations in plage contrast will affect the determination of the chromospheric plages. The histogram method is more robust with respect to the variations in plage contrast.

Figure 1b shows example of plages and network elements identified via this procedure.

We define the plage index as the fraction of the solar hemisphere occupied by the chromospheric plages at any given time. In the following discussion, however, we describe only monthly and yearly averages of Ca II K plage index. Plage index is calculated by using plage areas corrected for foreshortening.

3. Comparison of the Three Data Sets and Discussion

The main purpose of this article is to describe the reduction procedure for digitized images accumulated at three different instruments over the period of many solar cycles. Although our reduction procedure follows a similar path of previous studies (*e.g.*, Foukal, 1996; Lefebvre *et al.*, 2005; Ermolli *et al.*, 2008), we use a different approach to identify the solar limb, subtract the large-scale intensity variations, photometrically calibrate images, and identify bright plages.

Figure 3 presents correlation plots of annually averaged Ca II K plage indices derived for the Mount Wilson Observatory data set using three different reduction techniques: UCLA data reduction (Lefebvre *et al.*, 2005), Apn index (Foukal, 1998), and a reduction routine developed by us (TPS thereafter). Overall, we see good general agreement among the three reduction techniques. The Spearman rank correlation between UCLA and TPS plage indices is $r_{\rm s} = 0.95$, and for Apn – TPS indices, $r_{\rm s} = 0.94$. In both cases, the correlation is statistically significant, with the probability of no correlation at the extremely low level of about 10^{-37}. For an additional discussion of Ca II K plage indices computed using these three different methods we refer the reader to the accompanying paper by Foukal *et al.* (2009).

Figures 4 and 5 show correlation plots between monthly averaged plage indices for MWO, KKL, and NSO/SP data. Each solar cycle shows a reasonably good linear correlation between plage indices derived from different data sets. The average slope b of the functional dependence between MWO and KKL monthly plage indices is about 0.8, whereas

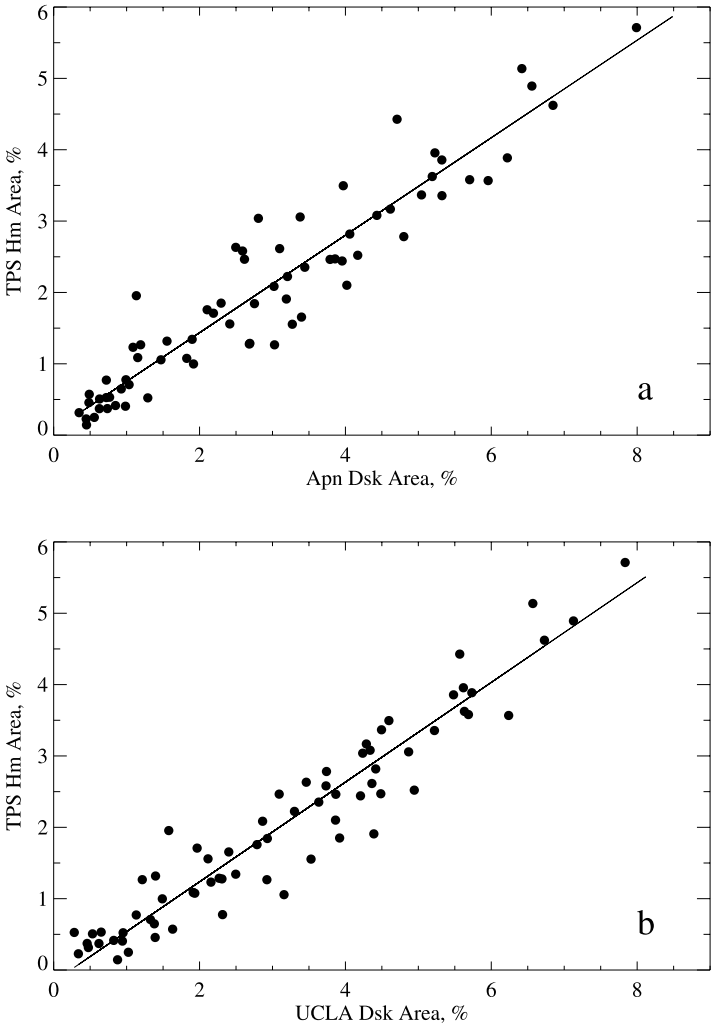

Figure 3 Relationship between annual Ca II K plage indices derived using MWO data set and three different reduction techniques: Apn (Foukal, 1998), UCLA (Lefebvre *et al.*, 2005), and by us (TPS). Apn and UCLA plage indices are expressed in units of fraction of visible solar disk, DSK; TPS plage index is in units of fraction of solar hemisphere, Hm. The solid line shows the first-degree polynomial approximation to the data.

the slope between MWO and NSO/SP data is about unity. In solar cycle 19, however, the slope between MWO and KKL data is significantly smaller ($b = 0.57$). A smaller slope is also observed in cycle 18 data, although to a lesser degree than in cycle 19.

Several effects may influence the slope of correlation plots shown on Figures 4 and 5. For example, data taken with off-band or a broader exit slit would increase the contribution of the photospheric light and hence are expected to result in a reduced area of the chromospheric plages. However, the narrow-band images should exhibit a tendency for larger plage areas as well as a larger contrast of plages with respect to the surrounding chromosphere.

To test this hypothesis, we have computed a plage brightness per unit area, or plage contrast, $P_{\rm con}$. Figure 6 shows variations of $P_{\rm con}$ for instruments in our data set.

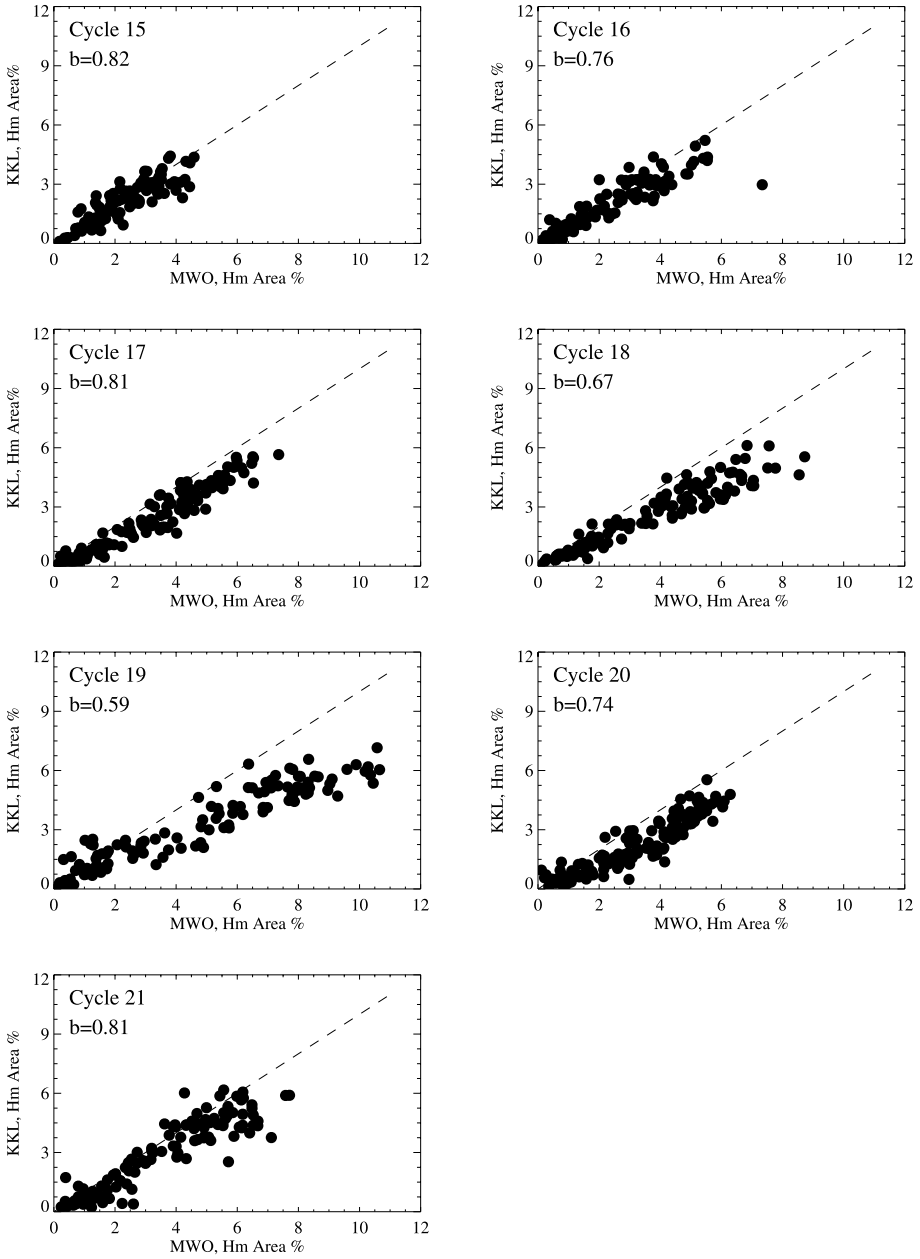

Figure 4 Relationship between the monthly averaged Ca II K plage indices derived using MWO and KKL data for different solar cycles. The dashed line shows a loci of a perfect agreement. Also shown on each panel is the slope (b) of a linear approximation for each subset. Note the significant change in slope ($b = 0.57$) for solar cycle 19.

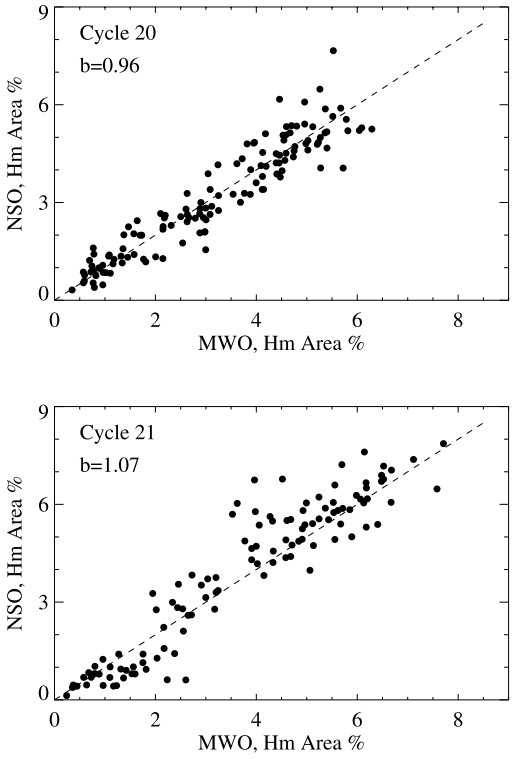

Figure 5 Same as Figure 4, but for NSO/SP and MWO data sets.

The mean plage contrast in KKL data is about 1.33 ± 0.10 and it shows very little variation throughout the data set. The average $P_{\rm con}$ for the MWO data set is slightly larger, 1.50 ± 0.20. A higher contrast in MWO data is in agreement with the narrow-bandpass observations taken at MWO. The average plage brightness in MWO data is also relatively constant through the data set, with the exception of a period around solar cycle 19. The NSO/SP data set exhibits the highest value of $P_{\rm con} = 2.09 \pm 0.20$ as well as larger variations in plage contrast as compared with the MWO and KKL data. This high plage contrast is at odds with the fact that KKL and NSO/SP data were obtained with a similar bandpass of 0.5 Å.

The period of higher contrast in MWO data coincides with cycle 19 and with the period of low slope in the KKL – MWO correlation (Figure 4). Cycle 18, however, also exhibits a lower slope in the KKL – MWO correlation, despite the plage contrast being normal. Also, despite the higher contrast in NSO/SP data, the functional relation between NSO/SP and MWO data is about unity (Figure 5), which does not support the change in bandpass as the explanation for the low slope in the KKL – MWO correlation. The plage contrast itself could be explained by the photographic properties of film (*i.e.*, film contrast) used by different observatories in different years. However, this conjecture about the role of film contrast needs further investigation.

It is more likely that the abnormal behavior of cycles 18 and 19 can be explained by the masking effect of sunspots in calculation of plage indices. Because of their broader bandpass, KKL and NSO/SP spectroheliograms tend to show dark sunspots inside bright chromospheric plages. MWO data taken with a narrower spectral bandpass do not show sunspots as readily as KKL and NSO/SP data. The definition of plages excludes dark sunspots sit-

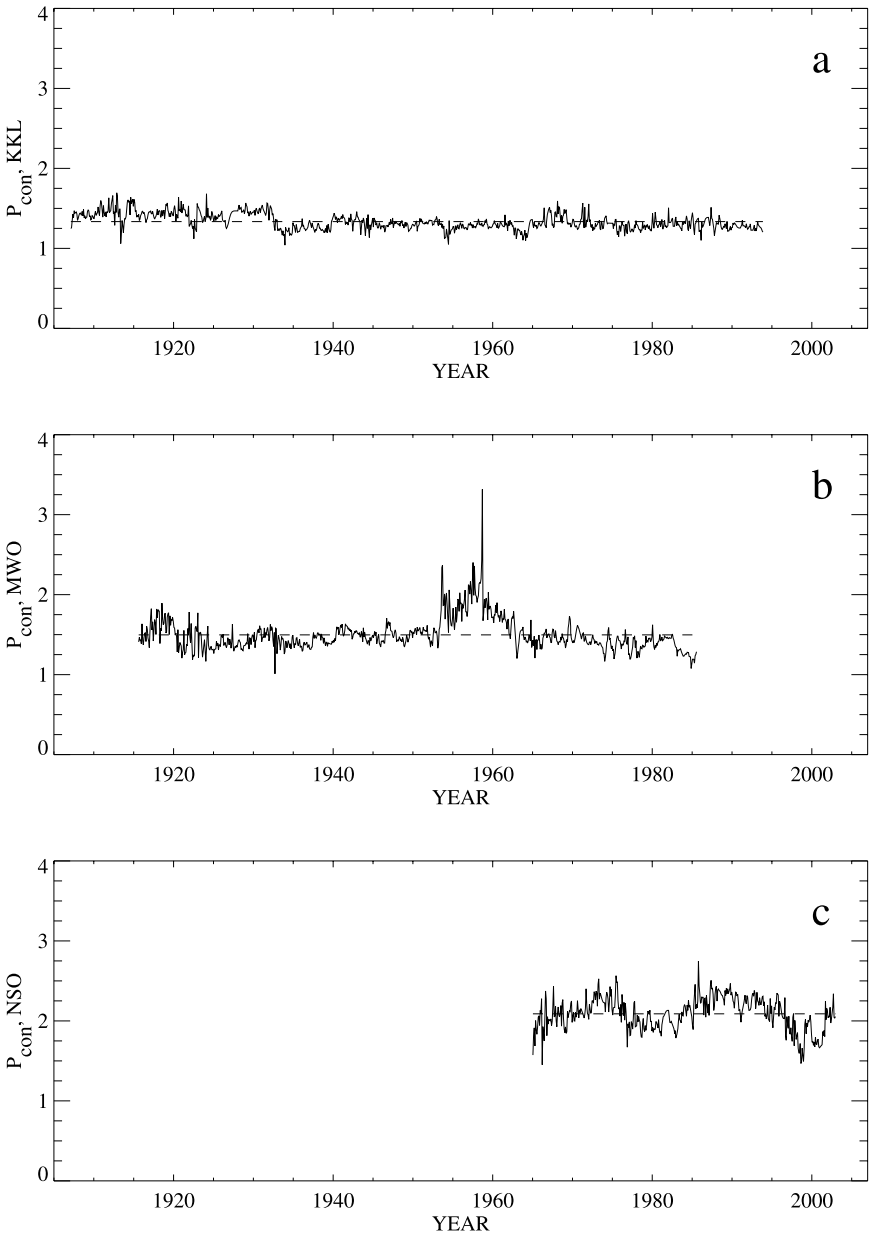

Figure 6 Average plage contrast, $P_{\rm con}$, relative to a quiet Sun's chromosphere for (a) the Kodaikanal, (b) the Mount Wilson, and (c) the National Solar Observatory at Sacramento Peak. The dashed lines show the mean $P_{\rm con}$ for each data set.

uated inside bright plages, which reduces the area of plages. The effect is noticeable only when a significant number of (large) sunspots is present on the disk (*i.e.*, at around maxima of a few largest solar cycles). Both cycles 18 and 19 fall into this category. Figure 7 shows

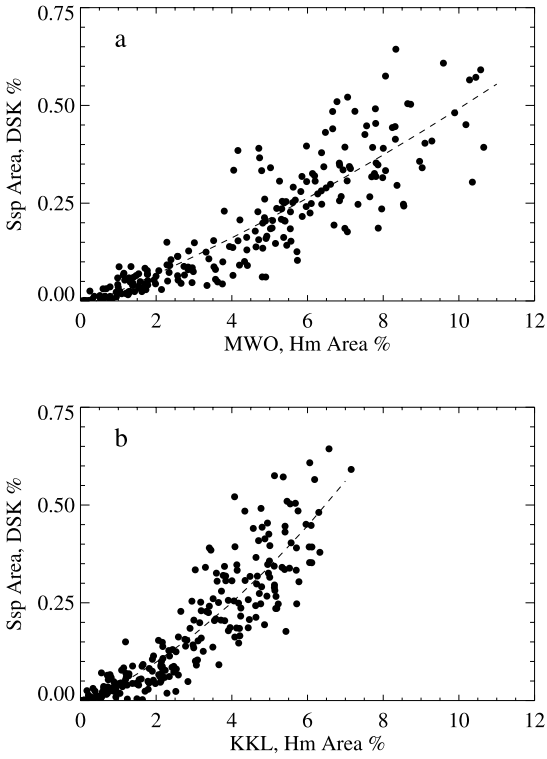

Figure 7 Monthly averaged sunspot area and plage index for solar cycles 18 and 19 for (a) the Mount Wilson and (b) the Kodaikanal Observatories. The dashed line shows a second-degree polynomial approximation.

monthly averaged sunspot area (from the Greenwich Heliophysical Observatory) and the plage index for solar cycles 18 and 19 for MWO and KKL data. A quadratic fit to the data ($S_{\rm area} = A + Bx + Cx^2$, where x is the plage index) indicates a much steeper dependency for KKL data ($C = 0.0055 \pm 0.0015$) as compared with MWO data ($C = 0.0011 \pm 0.0006$). We believe that this sunspot masking effect may be responsible for lowering the amplitude of maxima in solar cycles 18 and 19 in KKL and NSO/SP data as compared with MWO data. Foukal (1993) had considered such a sunspot masking effect in the relationship between the photospheric faculae and sunspot areas.

This discussion indicates how the photographic data from different observatories can be combined into a single data set. The reduction procedures including the one described in this paper allow correction and calibration of photographic data to achieve reasonable agreement among the different data sets. The remaining differences can be corrected by implementing the correlation and $P_{\rm con}$ plots shown here.

Because of difference in bandpass, KKL, NSO/SP, and MWO data sample different parts of solar atmosphere and, as the result, would approximate contributions to different parts of the UV spectra. We refer the reader to the accompanying paper (Foukal *et al.*, 2009) for additional discussion of this issue.

Overall, we find a good correlation between our monthly and yearly Ca II K indices and the international sunspot numbers (not shown). This high correlation provides an independent support for our data reduction procedure. However, it is worth noting that the Ca II K index can be useful for more than just reproducing the cyclic variation of solar activity derived from other known indices. For example, digitized Ca II K images may provide information on latitudinal variation of magnetic activity, especially in high latitudes, where no

other indices can contribute. As an example, we have recently used digitized Ca II K data to study high-latitude magnetic activity as a precursor for sunspot activity in mid and low latitudes. The results of this study will be published in a separate paper in the near future.

Acknowledgements We are thankful to Drs. L. Bertello and P. Foukal for providing UCLA-reduced and Apn data sets for comparison with our data reduction technique. The work of A.G.T. was supported by the Russian Foundation for Basic Research (RFBR) and a research program of the Presidium of the Russian Academy of Sciences (RAS). The National Solar Observatory is operated by the Association of Universities for Research in Astronomy, AURA, Inc., under a cooperative agreement with the National Science Foundation. The international sunspot numbers used in this paper are produced by the SIDC, RWC Belgium, World Data Center for the Sunspot Index, Royal Observatory of Belgium. The authors thank Ms. Jackie Diehl for her help in preparation of the manuscript. We also thank the anonymous referee for constructive comments.

References

Ermolli, I., Tlatov, A., Solanki, S.K., Krivova, N.A., Singh, J.: 2007, In: Heinzel, P., Dorotovic, I., Rutten, R.J. (eds.) *The Physics of Chromospheric Plasmas, Astron. Soc. Pac.* **CS-368**, 53.

Ermolli, I., Solanki, S.K., Tlatov, A.G., Krivova, N.A., Ulrich, R.K., Singh, J.: 2008, arXiv:0802.3806.

Foukal, P.: 1993, *Solar Phys.* **148**, 219.

Foukal, P.: 1996, *Geophys. Res. Lett.* **23**, 2169.

Foukal, P.: 1998, *Geophys. Res. Lett.* **25**, 2909.

Foukal, P., Bertello, L., Livingston, W., Pevtsov, A.A., Singh, J., Tlatov, A.G., Ulrich, R.K.: 2009, *Solar Phys.* DOI:10.1007/s11207-009-9330-0.

Lefebvre, S., Ulrich, R.K., Webster, L.S., Varadi, F., Javaraiah, J., Bertello, L., Werden, L., Boyden, J.E., Gilman, P.: 2005, *Mem. Soc. Astron. Ital.* **76**, 862.

Makarov, V.I., Tlatov, A.G.: 2002, In: Makarov, V.I., Obridko, V.N. (eds.) *Solar Activity and Cosmic Rays after Polar Field Polarity Reversal, Proc. 6th Int. Pulkovo Conf.*, 311 (in Russian).

Makarov, V.I., Tlatov, A.G., Singh, J., Gupta, S.S.: 2004, In: Stepanov, A.V., Benevolenskaya, E.E., Kosovichev, A.G. (eds.) *Multi-Wavelength Investigations of Solar Activity, Proc. IAU Symp.* **223**, 125.

Ortiz, A., Rast, M.: 2005, *Mem. Soc. Astron. Ital.* **76**, 1018.

Pierce, A.K., Slaughter, C.D.: 1977, *Solar Phys.* **51**, 25.

Tlatov, A.G., Pevtsov, A.A.: 2005, In: Stepanov, A.V., Solov'ev, A.A., Dergachev, V.A. (eds.) *Solar Activity as a Factor in Space Weather, Proc. IX Pulkovo Int. Conf.*, 477 (in Russian).

Xie, Y., Ji, Q.: 2002, In: *16th Int. Conf. on Pattern Recognition* **2**, 957. DOI:10.1109/ICPR.2002.1048464.